



Article

Role of metal atom doping on the transport properties of zigzag graphene nanoribbon with a vacancy defect

Gofur B.Eshonqulov ¹ , Anora Meylieva ¹ , Golibjon R.Berdiyrov ^{2*}

¹ Department of Physics, National University of Uzbekistan, Tashkent, 100174, Uzbekistan

² Qatar Environment and Energy Research Institute, Hamad Bin Khalifa University, Doha, 5825, Qatar
gberdiyrov@hbku.edu.qa

* Correspondence: gberdiyrov@hbku.edu.qa; Tel.: +974 44546704.

Abstract:

Graphene nanoribbons (GNRs) with structural defects have attracted significant interest due to their tunable electronic and magnetic properties. In this study, we investigate the role of transition metal (Co and Fe) doping on the transport properties of zigzag GNRs containing single vacancy defects, terminated either by unsaturated carbon atoms or pyridinic nitrogen atoms. Using density functional theory (DFT) combined with non-equilibrium Green's function formalism, we analyze the electronic transport characteristics and spin-dependent effects. Our findings reveal that metal atom doping has a contrasting impact depending on the defect type: in carbon-terminated vacancies, metal atoms reduce conductivity due to enhanced localization of electronic states, while in pyridinic defects, they enhance conductivity by extending transmission states. Additionally, metal doping significantly improves spin filtering efficiency, making doped GNRs promising for spintronic applications. These results emphasize the importance of defect engineering in graphene-based nanodevices and provide insights into optimizing electronic transport properties through selective doping strategies.

Keyword: graphene nanoribbons, transition metal doping, vacancy defects, spin transport, electronic conductivity, density functional theory.

Introduction

Graphene is undoubtedly the most promising 2D material for practical applications, primarily due to its mechanical and thermal stability, as well as its exceptionally high carrier mobility and flux [1, 5]. The ballistic nature of electronic transport makes graphene one of the best-suited materials for high-frequency applications [6,10]. Chemically processed synthesized graphene typically isn't perfect; it often contains various structural imperfections like grain boundaries, vacancies, dislocations, impurity atoms, and defects associated with changes in carbon hybridization [11,14]. It is known that these defects significantly alter the structural, electronic, optical, and other observable characteristics of graphene [15,17]. This sensitivity arises from the fact that even minor alterations in the honeycomb arrangement of carbon atoms can have a profound impact on these properties. They also influence the absorption of both metallic and non-metallic atoms/molecules onto graphene. For instance, metals and metal oxides tend to deposit primarily at defective sites on graphene [18,19]. Defects impede the clustering of transition metals [20] but promote the adsorption of certain reagents, such as thiol and hydroxyl radicals, by generating new active sites [21,22]. In turn, these metal inclusions profoundly influence the physical and chemical properties of graphene and by altering the electronic environment, they enhance the material's catalytic, electronic, and mechanical properties, thereby broadening its range of applicability in various technologies [23,29]. This modification not only tailors graphene for specific applications but also potentially unlocks new functionalities, making it even more versatile and valuable in fields ranging from electronics to energy storage and conversion.

On the other hand, certain impurities can be used to enhance the functionality of graphene. For example, Nitrogen (N) plays an important role as a dopant impurity in tuning the conductivity by

Quoting: G.B. Eshonqulov, A. Meylieva, G.R. Berdiyrov. Role of metal atom doping on the transport properties of zigzag graphene nanoribbon with a vacancy defect. 2024, 1,2, 1. <https://doi.org/>

Received: 10.12.2024

Corrected: 18.12.2024

Accepted: 25.12.2024

Published: 30.12.2024

Copyright: © 2024 by the authors. Submitted to for possible open access publication under the terms and conditions of the Creative Commons Attribution (CC BY) license (<https://creativecommons.org/licenses/by/4.0/>).

introducing additional electrons, which are released from pentavalent nitrogen atoms substituting tetravalent carbon atoms [30,33]. Graphene can exhibit three distinct types of nitrogen doping: pyridinic, pyrrolic, and graphitic [30]. Graphitic nitrogen directly substitutes carbon atoms within the graphitic lattice, potentially leading to the formation of an n-type conductor [34]. Pyridinic nitrogen forms bonds with two carbon atoms within a hexagonal structure, whereas pyrrolic nitrogen bonds with two carbon atoms arranged in a pentagonal configuration. These nitrogen types are frequently found at the edges of the layer but may also occur within the layer, often in conjunction with vacancies. Incorporating metal atoms into nitrogen-substituted defects further citeines the functionality of graphene and broadens its potential applications [35,37]. These defects can further tailor the magnetic properties of graphene [38,40], with potential implications in spintronics, magnetic storage, and nanoscale sensing.

In this study, we study the spin-dependent electronic transport properties of zigzag graphene nanoribbon (GNR) with vacancy defects, terminated either with unsaturated carbon or pyridinic nitrogen atoms (see Fig. 1), using the density functional theory (DFT) in combination with non-equilibrium Green's function formalism. Our findings reveal a decrease in conductivity after nitrogen substitution. Additionally, we investigate the effect of metal atoms embedded within the vacancy defects on the electronic transport properties of the GNR. The effect of metal atoms strongly depends on the nature of the vacancy defect: while metal atoms decrease conductivity in carbon-terminated defects, they result in enhanced conductivity in pyridinic defects. The obtained current reduction in the former case stems from the the localization of electronic states, as elucidated through analysis of the energy-dependent transmission eigenstates.

Materials and Methods

Our model systems consist of hydrogen terminated zigzag GNR with a single vacancy defect, which is terminated either with unsaturated carbon bonds (GNR-C sample; see Fig. 1 (a)) or by nitrogen atoms (i.e., pyridinic N3-vacancy; GNR-N sample; see Fig. 1 (c)). Transition metal (M) atoms are incorporated within these vacancy defects through covalent M-C and M-N bonds, as shown in Figures 1 (b, d). The size of the electrodes in these device geometries is 4.95 Å and the size of the central region is 6 times larger than the electrode size. As a reference, we also investigate the transport properties of pristine GNR with electrodes of the same length.

The device structures are geometry optimized using Density Functional Theory (DFT) within the Perdew-Burke-Ernzerhof (PBE) generalized gradient approximation for exchange-correlation energy [41], following the optimization procedure described in Ref. [42]. The Grimme's PBE empirical correction [43] is employed to consider non-bonded van der Waals interactions, while Brillouin zone integration is conducted using a $1 \times 1 \times 500 \times$ Monkhorst-Pack mesh [44] for k-points sampling. All atoms are characterized using norm-conserving PseudoDojo pseudopotentials with a medium basis set [45]. In the simulations, the convergence criterion for Hellmann-Feynman forces was set at 0.01 eV/Å, and the density mesh cut-off energy was established at 2176.91 eV.

The current-voltage (I-V) characteristics of the considered systems are computed utilizing the nonequilibrium Green's function formalism [46] within the Landauer-Büttiker approach:

$$I(V) = \frac{2e}{h} \int_{\mu_L}^{\mu_R} T(E, V) [f(E - \mu_L) - f(E - \mu_R)] dE, \quad (1)$$

where $T(E, V)$ represents the transmission spectrum at a specific applied voltage (V), $f(E, E_F)$ denotes the Fermi-Dirac distribution function, and μ_L/μ_R stand for the chemical potential of the left/right electrode, respectively. The transmission coefficients are obtained from

$$T(E, V) = T_{LR}(E, V) G_C(E, V) T_{LL}(E, V) G_C^\pm(E, V), \quad (2)$$

where $G_C(E, V)$ and $G^+(E, V)$ denoted the retarded Green's function for the active region and $\Gamma_{L/R}(E, V)$ are the coupling coefficients for the left/right electrodes, respectively. The computational package *Atomistix Toolkit* [47,48] is employed for conducting the calculations.

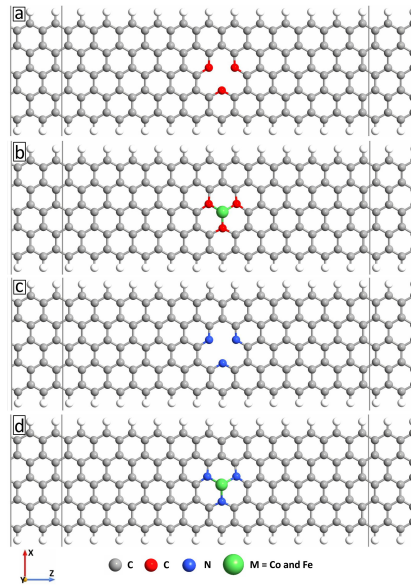


Figure 1. Device geometries consisting of 10 carbon atoms wide zig-zag graphene nanoribbon with C-terminated (a) and N-terminated (c) vacancy defects without (a,c) and with (b,d) transition metal (Co and Ni) atoms.

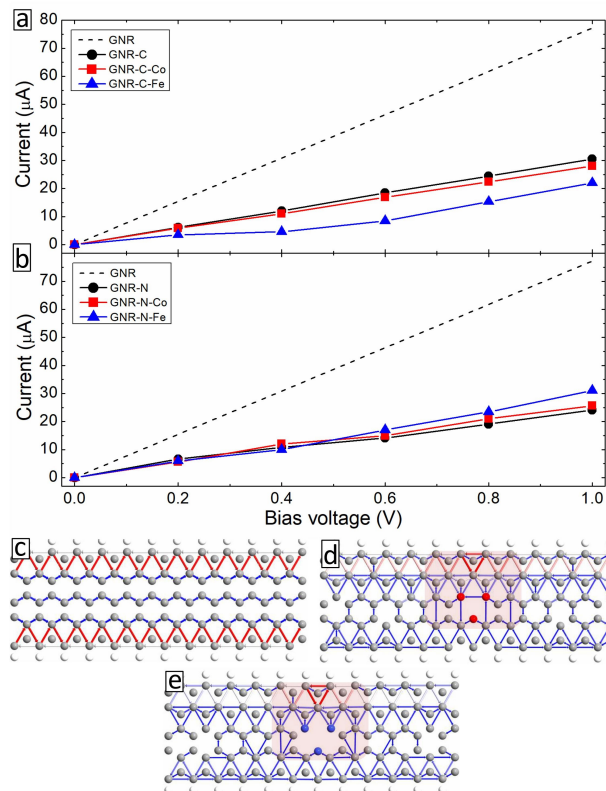


Figure 2. (a,b) Current-voltage characteristics of zigzag GNR with C-terminated (a) and N-terminated (b) vacancy defect without and with transition metal atoms (Co and Fe). Dashed curves show the results for the pristine GNR. (c-e) Zero voltage transmission pathways for pristine GNR (c), GNR with a vacancy defect (d) and GNR with pyridinic N3-vacancy (e). Defect areas are highlighted.

Results

We begin by analyzing the I-V characteristics of the system with C-terminated vacancy defect (see Fig. 1 (a)). The dashed curve shows the I-V curve of the pristine GNR, where the current

increases linearly with applied voltage. The presence of the vacancy defect decreases the current through the system by more than a factor of 2 (black circles in Fig. 2 (a)), due to the backscattering of electrons from the vacancy defect. This is shown in Fig. 1(d), which shows the transmission pathways at zero bias voltage. The attachment of the metal atoms at the vacancy defect decreases the current through the sample for any given value of the applied voltage, with the smallest current for the Iron (Fe) atom (blue triangles). More than 50 % decrease in the current is obtained depending on the applied voltage. To identify the origin for the reduced current after metal atom embedment, we conducted analysis of device density of states (DDOS), transmission spectra ($T(E)$), and transmission eigenstates for the considered systems. Figure 3 shows the DDOS (a) and $T(E)$ (b) as a function of electron energy for GNR-C (solid-black curves) and GNR-C-Fe samples (dashed-red curves) at bias voltage 0.6 V for which we obtained the largest reduction of the current due to metal atom attachment. Despite smaller DDOS, the electron transmission at the Fermi level is larger for the GNR-C sample with extended transmission eigenstates (see panel 1 in Fig. 3). The metal atom incorporation results in strong localization of the electronic states (see panel 2) which reduces the transmission probability of the electrons through the junction. Similar effect of the metal atom is also obtained for the other electron energies (see panels 3 and 4). Thus, the reduced current in the samples with metal atom inclusions are related to nanoscale charge localization on the system.

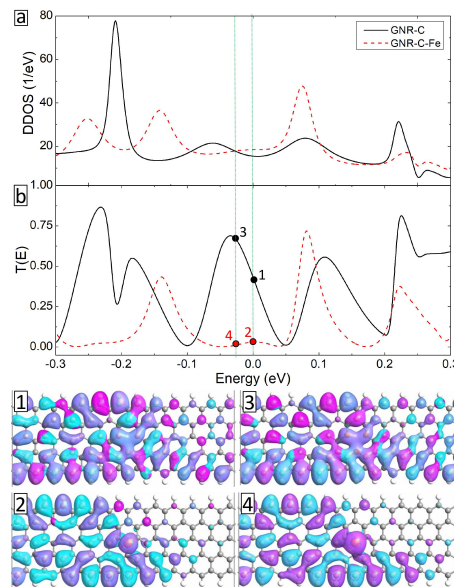


Figure 3. Device density of states (a) and transmission spectra (b) as a function of electron energy (zero corresponds to the Fermi level) for GNR-C (solid-black curves) and GNR-C-Fe (dashed-red curves) samples at bias voltage 0.6 V. Panels 1-4 show the isosurface plots (*isovalue* $0.1 \text{ \AA}^{-1.5} \text{ eV}^{-0.5}$) of transmission eigenstates of sample GNR-C (panels 1 and 3) and GNR-C-Fe (panels 2 and 4) at electron energies indicated on the transmission curves.

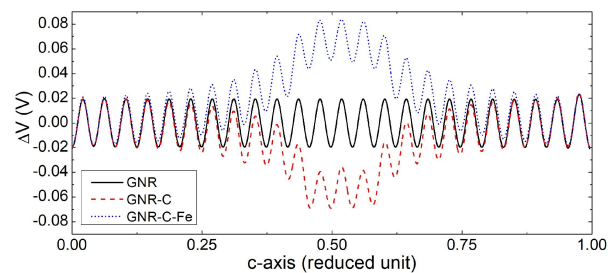


Figure 4. Variations of averaged electrostatic difference potential for pristine GNR (solid-black curve), GNR-C (dashed-red curve) and GNR-C-Fe (dotted-blue curve) samples at zero bias voltage.

Another important factor that affects the electronic transport properties of low-dimensional materials [49] is the variations of the electrostatic potential. Therefore, we plot in Fig.4 the variations of the electrostatic difference potential (ΔV) in pristine GNR (solid-black curve), GNR-C (dashed-red curve) and GNR-C-Fe (dotted-blue curve) samples. This quantity is determined by subtracting the electrostatic potential of the self-consistent valence charge density (i.e., solution of the Poisson equation) from the potential obtained through the superposition of atomic valence densities. ΔV of pristine GNR is characterized by periodic oscillation with amplitude 0.04 V. The vacancy defect creates a significant potential barrier for electrons in the middle of the sample, which can account for the reduced current observed in this system. The presence of the metal atom further increases this barrier which further decreases the current. This observation may provide an explanation for the reduced current observed after the incorporation of metal atoms.

Next, we consider the case when the carbon atoms at the defect edge are substituted by nitrogen atoms (see Fig. 1 (b)). The presence of the pyridinic defect also reduces the current of the pristine GNR (solid-black curve in Fig. 2 (b)). It is interesting to note that the incorporation of a metal atom enhances the current in the system for this type of defect. To find the origin of the enhanced current after metal atom embedment, we plot in Fig. 5 DDOS (a) and $T(E)$ (b) as a function of electron energy at bias voltage 0.6 V for GNR-N (solid-black curves) and GNR-N-Fe samples (dashed-red curves). The DDOS of the former system exhibits an almost constant value across the considered range of electron energy, with the exception at larger electron energies. Despite smaller DDOS, the system with metal atoms show larger transmission for most of the electron energies. In addition, the electronic states becomes extended over the junction, which, consequently, enhances the current across the sample.

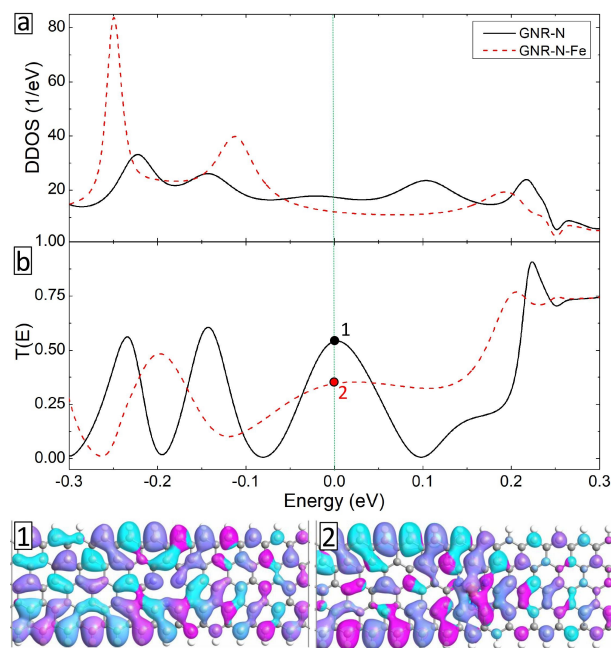


Figure 5. Device density of states (a) and transmission spectra (b) as a function of electron energy (zero corresponds to the Fermi level) for GNR-N (solid-black curves) and GNR-N-Fe (dashed-red curves) samples at bias voltage 0.6 V. Panels 1 and 2 show the isosurface plots (*isovalue* $0.1 \text{ \AA}^{-1.5} \text{ eV}^{-0.5}$) of transmission eigenstates of sample GNR-N (panels 1) and GNR-N-Fe (panels 2) at the Fermi level.

It is known that reconstructed vacancy defects containing carbon atoms with unsaturated bonds, behave like quasilocalized magnetic impurities [50]. In what follows we study how the metal atom embedment affect the spin-filtration potential of the graphene. For that purpose, we plot in Fig. 6 the ratios of currents (i.e., asymmetry) for spin-up and spin-down electrons for both C-terminated (a) and N-terminated (b) vacancy defects. As expected, the pristine GNR shows no asymmetry in the current. The presence of the vacancy defects results in a larger current for spin-up electrons, but

the value of the asymmetry does not exceed 3 % (black circles in Fig. 6 (a)). The presence of the ferromagnetic atoms increases the spin filtration property of the system with maximum asymmetry (61 %) for the Co atom (red squares in Fig. 6 (a)). The Fe atom also shows the enhanced spin filtration (blue triangles in Fig. 6 (a)). The effect of the metal atoms on the spin-dependent electronic transport becomes more pronounced for the system with pyridinic vacancy defect (Fig. 6 (b)): the asymmetry increase by a factor of 2 for both Co and Fe atoms (red squares and blue triangles). The pristine GNR-N sample also shows enhanced spin filtration (13 %; black circles). Thus, pyridinic vacancy defects are more effective in enhancing the spin selectivity of graphene.

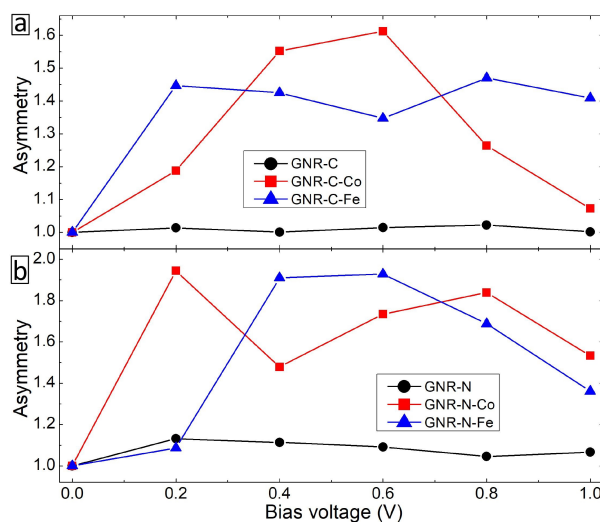


Figure 6. Asymmetry (i.e., ratio of currents for spin up and spin down electrons) as a function of bias voltage for the system with C-terminated (a) and N-terminated (b) vacancy defects without and with metal atoms.

Conclusions

Using density functional theory in combination with the nonequilibrium Greens functional formalism, we study the effects of different vacancy defects and metal dopants on the spin-dependent transport properties of zigzag graphene nanoribbons. We found that pyridinic nitrogen atoms reduce the conductivity of GNR as compared to C-terminated vacancy defects. The influence of metal atoms varies depending on the defect type, increasing conductivity in pyridinic defects but reducing it in C-terminated defects. Additionally, the pyridinic system exhibits enhanced spin dependency in charge transport, suggesting potential advantages for spintronic nanodevices. These findings show the importance of defect engineering and dopant selection in graphene device design and highlight avenues for future research in understanding and utilizing graphene-based devices.

Authors' contribution.

Conceptualization, G.E. and G.B.; methodology, G.E.; software, A.M.; validation, G.E., A.M., and G.B.; formal analysis, G.E.; investigation, G.E.; resources, G.B.; data curation, A.M.; writing—original draft preparation, G.E.; writing—review and editing, G.B.; visualization, A.M.; supervision, G.B.; project administration, G.E.; funding acquisition, G.B. All authors have read and agreed to the published version of the manuscript.

Funding source.

The Agency for Innovative Development of the Republic of Uzbekistan (Grant number FZ-2020092435).

Ethics approval.

Not applicable. This study did not involve humans or animals.

Consent for publication.

Not applicable. This study did not involve human participants, and therefore, informed consent was not required.

Data Availability Statement

The data supporting the reported results are available upon reasonable request from the corresponding author. No publicly archived datasets were used in this study.

Acknowledgments

The authors would like to thank the National University of Uzbekistan for providing computational resources and administrative support. We also appreciate the technical assistance from the Qatar Environment and Energy Research Institute (QEERI) at Hamad Bin Khalifa University. Additionally, we acknowledge the valuable discussions and insights provided by our colleagues in the Department of Physics at the National University of Uzbekistan.

Conflict of interest

The authors declare no conflicts of interest. The funders had no role in the design of the study; in the collection, analyses, or interpretation of data; in the writing of the manuscript; or in the decision to publish the results.

Abbreviations

GNR	Graphene Nanoribbon
DFT	Density Functional Theory
PBE	Perdew-Burke-Ernzerhof
DOS	Density of States
Co	Cobalt
Fe	Iron
N	Nitrogen
I-V	Current-Voltage
DDOS	Device Density of States
T(E)	Transmission Spectrum

References

- [1] K. S. Novoselov, A. K. Geim, S. V. Morozov, D. Jiang, Y. Zhang, S. V. Dubonos, I. V. Grigorieva, A. A. Firsov, Electric field effect in atomically thin carbon films, *Science* 306 (2004) 666.
- [2] A. K. Geim, K. S. Novoselov, The rise of graphene, *Nature Mater.* 6 (2007) 183.
- [3] A. K. Geim, Graphene: Status and Prospects, *Science* 324 (2009) 1530-1534.
- [4] A. H. Castro Neto, F. Guinea, N. M. R. Peres, K. S. Novoselov, A. K. Geim, The electronic properties of graphene, *Rev. Mod. Phys.* 81 (2009) 109.
- [5] K. S. Novoselov, V. I. Fal'ko, L. Colombo, P. R. Gellert, M. G. Schwab, K. Kim, A roadmap for graphene, *Nature* 490 (2012) 192.
- [6] L. Vicarelli, M. S. Vitiello, D. Coquillat, A. Lombardo, A. C. Ferrari, W. Knap, M. Polini, V. Pellegrini, A. Tredicucci, Graphene field-effect transistors as room-temperature terahertz detectors, *Nature Mater.* 11 (2012) 865-871.
- [7] G. Auton, D. B. But, J. Zhang, E. Hill, D. Coquillat, C. Consejo, P. Nouvel, W. Knap, L. Varani, F. Teppe, J. Torres, A. Song, Terahertz Detection and Imaging Using Graphene Ballistic Rectifiers, *Nano Lett.* 17 (2017) 7015-7020.
- [8] D. A. Bandurin, D. Svintsov, I. Gayduchenko, S. G. Xu, A. Principi, M. Moskotin, I. Tretyakov, D. Yagodkin, S. Zhukov, T. Taniguchi, K. Watanabe, I. V. Grigorieva, M. Polini, G. N. Goltsman, A. K. Geim, G. Fedorov, Resonant terahertz detection using graphene plasmons, *Nat. Commun.* 9 (2019) 5392.
- [9] G. R. Berdiyev, H. Hamoudi, Creating graphene geometry diodes through fluorination: First-principles studies, *Comput. Mater. Sci.* 188 (2021) 110209.
- [10] M. Andelkovic, Kh. Yu. Rakhimov, A. Chaves, G. R. Berdiyev, M. V. Milošević, Wave-packet propagation in a graphene geometric diode, *Physica E* 147 (2023) 115607.
- [11] M. H. Gass, U. Bangert, A. L. Bleloch, P. Wan, R. R. Nair, A. K. Geim, Free-standing graphene at atomic resolution, *Nat. Nanotechnol.* 3 (2008) 676-681.
- [12] J. C. Meyer, C. Kisielowski, R. Erni, M. D. Russell, M. F. Crommie, A. Zettl, Direct Imaging of Lattice Atoms and Topological Defects in Graphene Membranes, *Nano Lett.* 8 (2008) 3582-3586.

- [13] A. Eckmann, A. Felten, A. Mishchenko, L. Britnell, R. Krupke, K. S. Novoselov, C. Casiraghi, Probing the Nature of Defects in Graphene by Raman Spectroscopy, *Nano Lett.* 12 (2012) 3925-3930.
- [14] U. Khalilov, M. Yusupov, G.B. Eshonqulov, E.C. Neyts, G.R. Berdiyrov, Atomic level mechanisms of graphene healing by methane-based plasma radicals, *FlatChem* 39 (2023) 100506.
- [15] A. Hashimoto, K. Suenaga, A. Gloter, K. Urita, S. Iijima, Direct evidence for atomic defects in graphene layers, *Nature* 430 (2004) 870.
- [16] F. Banhart, J. Kotakoski, A. V. Krasheninnikov, Structural Defects in Graphene, *ACS Nano* 5 (2011) 26-41.
- [17] R. H. Telling, M. I. Heggie, Radiation defects in graphite, *Philos. Mag.* 87 (2007) 4797-4846.
- [18] X. Wang, S. M. Tabakman, H. Dai, Atomic Layer Deposition of Metal Oxides on Pristine and Functionalized Graphene, *J. Am. Chem. Soc.* 130 (2008) 8152.
- [19] S. Malola, H. Hakkinen, P. Koskinen, Gold in graphene: in-plane adsorption and diffusion, *Appl. Phys. Lett.* 94 (2009) 043106.
- [20] A. V. Krasheninnikov, P. O. Lehtinen, A. S. Foster, P. Pyykko, R. M. Nieminen, Embedding Transition-Metal Atoms in Graphene: Structure, Bonding, and Magnetism, *Phys. Rev. Lett.* 102 (2009) 126807.
- [21] P. A. Denis, Density Functional Investigation of Thioepoxidated and Thiolated Graphene, *J. Phys. Chem. C* 113 (2009) 5612-5619.
- [22] N. Ghaderi, M. Peressi, First-Principle Study of Hydroxyl Functional Groups on Pristine, Defected Graphene, and Graphene Epoxide, *J. Phys. Chem. C* 114 (2010) 21625.
- [23] J. Narayan, K. Bezborah, Recent advances in the functionalization, substitutional doping and applications of graphene/graphene composite nanomaterials, *RSC Adv.* 14 (2024) 13413-13444.
- [24] G. R. Berdiyrov, H. Abdullah, M. Al Ezzi, G. V. Rakhmatullaeva, H. Bahlouli, N. Tit, CO₂ adsorption on Fe-doped graphene nanoribbons: First principles electronic transport calculations, *AIP Adv.* 6 (2016) 125102.
- [25] G. R. Berdiyrov, H. Bahlouli, F. M. Peeters, Effect of substitutional impurities on the electronic transport properties of graphene, *Physica E* 84 (2016) 22-26.
- [26] A. Kanzariya, S. Vadalkar, S. K. Jana, L.K. Saini, P. K. Jha, An ab-initio investigation of transition metal-doped graphene quantum dots for the adsorption of hazardous CO₂, H₂S, HCN, and CNCl molecules, *J. Phys. Chem. Solids* 186 (2024) 111799.
- [27] E. T. Sayed, J. B.M. Parambath, M. A. Abdelkareem, H. Alawadhi, A.G. Olabi, Ni-based metal organic frameworks doped with reduced graphene oxide as an effective anode catalyst in direct ethanol fuel cells, *J. Alloys Compd.* 976 (2024) 173194.
- [28] F. Boltayev, G.B. Eshonqulov, G.R. Berdiyrov, Electronic transport calculations for CO₂ adsorption on calcium-decorated graphene nanoribbons, *Comput. Mater. Sci.* 145 (2018) 134-139.
- [29] T. Kousar, M. Aadil, S. Zulfiqar, S. M. Ibrahim, S. Mubeen, W. Hassan, K. Shafiq, F. Mahmood, Facile synthesis of graphene anchored rare earth doped mixed metal ferrite nanorods: A potential candidate for azo dye mineralization, *J. Rare Earths* 42 (2024) 907-916.
- [30] M. Inagaki, M. Toyoda, Y. Soneda, T. Morishita, Nitrogen-doped carbon materials, *Carbon* 132 (2018) 104-140.
- [31] M. Datt Bhatt, H. Kim, G. Kim, Various defects in graphene: a review, *RSC Adv.* 12 (2022) 21520.
- [32] R. Saini, F. Naaz, A. H. Bashal, A. H. Pandit, U. Farooq, Recent advances in nitrogen-doped graphene-based heterostructures and composites: mechanism and active sites for electrochemical ORR and HER, *Green Chem.* 26 (2024) 57-102.
- [33] M. A. Olgar, S. Erkan, A. Altuntepe, R. Zan, Nitrogen doped single layer graphene for CZTS-based thin film solar cells, *Opt. Mater.* 150 (2024) 115167.
- [34] O. Stephan, P. Ajayan, Doping graphitic and carbon nanotube structures with boron and nitrogen, *Science* 266 (1994) 1863-1865.
- [35] D. Rao, Y. Wang, Z. Meng, S. Yao, X. Chen, X. Shen, R. Lu, Theoretical study of H₂ adsorption on metal-doped graphene sheets with nitrogen-substituted defects, *Int. J. Hydrogen Energy* 40 (2015) 14154-14162.
- [36] L.-L. Liu, C.-P. Chen, L.-S. Zhao, Y. Wang, X.-C. Wang, Metal-embedded nitrogen-doped graphene for H₂O molecule dissociation, *Carbon* 115 (2017) 773-780.
- [37] A. Cho, B. J. Park, J. W. Han, Computational Screening of Single-Metal-Atom Embedded Graphene-Based Electrocatalysts Stabilized by Heteroatoms, *Front. Chem.* 10 (2022) 873609.
- [38] P. Esquinazi, D. Spemann, R. Höhne, A. Setzer, K.-H. Han, T. Butz, Induced Magnetic Ordering by Proton Irradiation in Graphite, *Phys. Rev. Lett.* 91 (2003) 227201.
- [39] S. Talapatra, P. G. Ganesan, T. Kim, R. Vajtai, M. Huang, M. Shima, G. Ramanath, D. Srivastava, S. C. Deevi, P. M. Ajayan, Irradiation-Induced Magnetism in Carbon Nanostructures, *Phys. Rev. Lett.* 95 (2005) 097201.

- [40] P. O. Lehtinen, A. S. Foster, A. Ayuela, T. T. Vehviläinen, R. M. Nieminen, Structure and magnetic properties of adatoms on carbon nanotubes, *Phys. Rev. B* 69 (2004) 155422.
- [41] J. P. Perdew, K. Burke, M. Ernzerhof, Generalized Gradient Approximation Made Simple, *Phys. Rev. Lett.* 77 (1996) 3865.
- [42] G. R. Berdiyrov, M. Alsalama, H. Hamoudi, Length-dependent high-frequency response of aromatic and aliphatic molecules: predictions from first-principles calculations, *J. Phys. Chem. Solids* 178 (2023) 111343.
- [43] S. Grimme, Semiempirical GGA-type density functional constructed with a long-range dispersion correction, *J. Comput. Chem.* 27 (2006) 1787-1799.
- [44] H. J. Monkhorst, J. D. Pack, Special points for Brillouin-zone integrations, *Phys. Rev. B* 13 (1976) 5188.
- [45] M. J. van Setten, M. Giantomassi, E. Bousquet, M. J. Verstraete, D. R. Hamann, X. Gonze, G.-M. Rignanese, The pseudodojo: Training and grading a 85 element optimized norm-conserving pseudopotential table, *Comput. Phys. Commun.* 226 (2018) 39-54.
- [46] M. Brandbyge, J. L. Mozos, P. Ordejón, J. Taylor, K. Stokbro, Density-functional method for nonequilibrium electron transport, *Phys. Rev. B* 65 (2002) 165401.
- [47] S. Smidstrup, T. Markussen, P. Vancraeyveld, J. Wellendorff, J. Schneider, T. Gunst, B. Verstichel, D. Stradi, P. A. Khomyakov, U. G. Vej-Hansen, QuantumATK: An integrated platform of electronic and atomic-scale modelling tools, *J. Phys.: Condens. Matter* 32 (2020) 015901.
- [48] S. Smidstrup, D. Stradi, J. Wellendorff, P. A. Khomyakov, U. G. Vej-Hansen, M.-E. Lee, T. Ghosh, E. Jonsson, H. Jonsson, K. Stokbro, First-principles Green's-function method for surface calculations: A pseudopotential localized basis set approach, *Phys. Rev. B* 96 (2017) 195309.
- [49] G. R. Berdiyrov, B. Mortazavi, H. Hamoudi, Anisotropic charge transport in 1D and 2D BeN₄ and MgN₄ nanomaterials: A first-principles study, *FlatChem* 31 (2022) 100327.
- [50] Z. Zanolli, J.-C. Charlier, Spin transport in carbon nanotubes with magnetic vacancy-defects, *Phys. Rev. B* 81 (2010) 165406.

Disclaimer of liability/Publisher's Note: The statements, opinions and data contained in all publications belong exclusively to individuals. The authors and participants, and the Journal and the editors. The journal and the editors are not responsible for any damage caused to people or property resulting from any ideas, methods, instructions or products mentioned in the content.